Thieme

Diagnosis and Differential Diagnosis of Hydrocephalus in Adults

Diagnostik und Differentialdiagnostik des Hydrocephalus beim Erwachsenen

Authors
Sönke Langner[1], Steffen Fleck[2], Jörg Baldauf[2], Birger Mensel[1], Jens Peter Kühn[1], Michael Kirsch[1]

Affiliation
1 Institute for Diagnostic Radiology and Neuroradiology, Universitymedicine Greifswald
2 Department of Neurosurgery, University Medicine Greifswald, Germany

Key words
hydrocephalus, brain, MR imaging

received 19.12.2016
accepted 15.03.2017

Bibliography
DOI https://doi.org/10.1055/s-0043-108550
Published online: 16.5.2017 | Fortschr Röntgenstr 2017; 189: 728–739 © Georg Thieme Verlag KG, Stuttgart · New York, ISSN 1438-9029

Correspondence
PD Dr. Sönke Langner
Institute for Diagnostic Radiology and Neuroradiology, Universitymedicine Greifswald, Ferdinand-Sauerbruch-Str. 1, 17475 Greifswald, Germany
Tel.: +49/38 34/86 69 60
Fax: +49/38 34/86 70 97
langso@uni-greifswald.de

ABSTRACT

Purpose Hydrocephalus is caused by an imbalance of production and absorption of cerebrospinal fluid (CSF) or obstruction of its pathways, resulting in ventricular dilatation and increased intracranial pressure. Imaging plays a crucial role in the diagnosis, differential diagnosis and planning of treatment.

Methods This review article presents the different types of hydrocephalus und their typical imaging appearance, describes imaging techniques, and discusses differential diagnoses of the different forms of hydrocephalus.

Results and Conclusion Imaging plays a central role in the diagnosis of hydrocephalus. While magnetic resonance (MR) imaging is the first-line imaging modality, computed tomography (CT) is often the first-line imaging test in emergency patients.

Key points

- Occlusive hydrocephalus is caused by obstruction of CSF pathways.
- Malabsorptive hydrocephalus is caused by impaired CSF absorption.
- The MR imaging protocol should always include sagittal high-resolution T2-weighted images.
- When an inflammatory etiology is suspected, imaging with contrast agent administration is necessary.

Citation Format

- Langner S, Fleck S, Baldauf J et al. Diagnosis and Differential Diagnosis of Hydrocephalus in Adults. Fortschr Röntgenstr 2017; 189: 728–739

ZUSAMMENFASSUNG

Ziel Bei einem „Hydrozephalus“ kommt es durch ein Missverhältnis zwischen Liquorproduktion und -resorption oder ein Abflusshindernis zu einer Dilatation der Ventrikel und einem konsekutiven Anstieg des Hirndrucks. Die Bildgebung ist von zentraler Bedeutung, um die Diagnose zu bestätigen, die Ursache zu identifizieren und die Therapie planen zu können.

Methode Der Übersichtsartikel stellt die verschiedenen Formen des Hydrozephalus und deren bildmorphologische Charakteristika vor, beschreibt die zur Verfügung stehenden Untersuchungstechniken sowie mögliche Differenzialdiagnosen der einzelnen Erkrankungen.

Ergebnisse und Schlussfolgerung Für die Diagnose und Differenzialdiagnose des Hydrozephalus ist die Bildgebung von zentraler Bedeutung. Untersuchungsmethode der Wahl ist die MRT wobei in Notfallsituationen die initiale Diagnostik häufig mit CT erfolgt.

This document was downloaded for personal use only. Unauthorized distribution is strictly prohibited.

Introduction

Hydrocephalus is a common symptom that can have a number of causes [1, 2]. However, if the symptom is not treated, hydrocephalus can develop into an independent disease that remains even after treatment of the cause and may require ongoing treatment.

In the past, analysis of the principles of CSF circulation has often been based on the Monro-Kellie doctrine [3]. According to this, the total volume of intracranial tissue (brain, CSF, arterial and venous blood) is constant due to the rigid dimensions. Since fluid cannot be compressed, an increase in volume in one compartment must be associated with a decrease in another compartment.

In the case of hydrocephalus, there is abnormal ventricular dilatation caused by an imbalance between CSF production and absorption [2]. Since the remaining intracranial tissue stays constant, there is an increase in intracranial pressure. This then results in transependymal CSF extravasation from the ventricular system into the brain parenchyma, leading to brain damage with corresponding symptoms [4] and to pressure-induced atrophy in the case of persistence of the disease [1]. A special form of hydrocephalus is known as "idiopathic normal pressure hydrocephalus".

In the case of clinical suspicion of hydrocephalus, imaging plays a central role in confirming the diagnosis, identifying the cause, and planning treatment.

This overview article presents the typical characteristics of hydrocephalus in cerebral imaging as well as common causes and their differential diagnoses in adults with their morphological imaging characteristics.

Anatomy and physiological basis

The ventricular system of the brain is comprised of the two lateral ventricles that can be divided into a frontal horn, the cella media as the central portion, and the trigone as the junction to the anterior horn and the temporal horn. There are also the unpaired third and fourth ventricles. The CSF volume is about 150 ml, and approximately 450 ml are produced each day, which means that the CSF is replaced three times a day [5]. In the classic CSF circulation model, known as the "bulk flow model" [6], the CSF is produced by the choroid plexus which is located primarily in the lateral ventricles and to a lesser extent also in the third ventricle and on the roof of the fourth ventricle. It runs from the lateral ventricles through the foramen of Monro into the third ventricle and from there through the aqueduct into the fourth ventricle. The fourth ventricle is connected to the subarachnoid spaces via the foramen of Magendie (median aperture) and the two lateral foramina of Luschka (lateral apertures). The external CSF spaces are divided into the basal cisterns and the external CSF spaces over the hemispheres. A further compartment is the spinal canal. CSF absorption occurs primarily via arachnoid granulations in the dural sinus and also to a lesser degree spinally [6]. However, current studies have shown that the physiology of CSF production and absorption is significantly more complex than previously assumed. Refer to the relevant overview articles for a more detailed discussion [7 – 10].

Clinical signs of hydrocephalus

The clinical manifestation depends on the etiology and the dynamics with which the hydrocephalus develops [11]. Acute, quickly developing hydrocephalus is a life-threatening disease requiring immediate neurosurgical treatment [4]. The acute increase in intracranial pressure can result in herniation of the temporal lobe through the tentorial notch, referred to as transtentorial herniation, and/or in herniation of the cerebellum into the foramen magnum. This can lead to a disorder of vigilance, disorder of pupil motor function and the oculomotor system, autonomic dysfunction, loss of brain stem reflexes and even coma. In contrast, slowly progressing chronic hydrocephalus often manifests with non-specific symptoms, such as headache, dizziness, and difficulties with vision and concentration. Additional typical clinical signs are vomiting in the morning and papilledema seen in the ophthalmological examination.

Examination methods and morphological imaging criteria of hydrocephalus

In patients with the clinical picture of acute hydrocephalus and acute impaired consciousness, cranial computed tomography is the primary examination method due to the shorter examination time and the faster access to the patient. Otherwise, the examination modality of choice is MRI [1, 12].

A typical sign of hydrocephalus is ventricular dilatation (▶ **Fig. 1**). A very sensitive sign of this is dilatation of the temporal horns. Even though there are no standard values for this in the literature, a diameter of > 2 mm in adults is considered pathological (▶ **Fig. 1**) [13]. Moreover, the width of the third ventricle increases so that it is no longer slit-shaped but rather ballooned or laterally bowed. The normally slit-shaped posterior horns also appear rounded. Compared to the dilated ventricular system, the external CSF spaces are disproportionately thin. Depending on the dynamics of the hydrocephalus, these changes can be very subtle and only able to be detected when comparing follow-up examinations.

The Evans' Index is used in the clinical routine to quantify dilatation of the ventricles in adults (▶ **Fig. 1**). A value of > 0.3 is considered pathological [14].

Transependymal CSF extravasation caused by the increase in pressure appears on cranial CT as hypodense changes in the region of the frontal and posterior horns. In MRI, these changes can be detected on T2-weighted (T2w) or ideally FLAIR scans (▶ **Fig. 2**). CSF extravasation must be differentiated from age-related changes of periventricular white matter [15]. Such changes are usually less than 10 mm in diameter on axial cross-sectional images (▶ **Fig. 2**) and their thickness decreases from anterior to posterior [16].

In the case of clinical suspicion of acute hydrocephalus, FLAIR scans are sufficient to rule out impaired CSF circulation and to detect or rule out CSF extravasation as an indirect sign of increased intracranial pressure. An MR imaging protocol (▶ **Table 1**) for diagnosis of the underlying cause in patients with confirmed hydrocephalus should always include high-resolution sagittal T2w scans (e. g. CISS method) [17]. T2w SPACE scans can be used as an alternative, particularly at 3 T [17]. The configuration

This document was downloaded for personal use only. Unauthorized distribution is strictly prohibited.

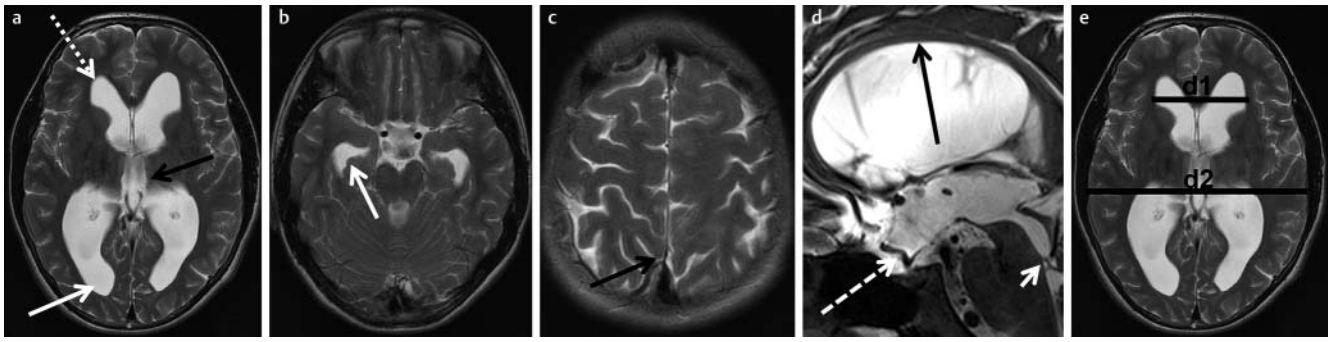

▶ **Fig. 1** Morphological imaging features of hydrocephalus. Axial T2w images of a 24-year-old woman with a 2-week history of headache, nausea and vomiting due to congenital aqueductal occlusion. The example illustrates the typical imaging findings of occlusive hydrocephalus. Increased pressure leads to ballooning of the frontal horns (dotted arrow in **a**), rounding of the posterior horn (arrow in **b**), dilatation of the temporal horns (arrow in **c**); and upward bowing and thinning of the corpus callosum (black arrow in **d**). The infundibular recess is also dilated (dotted arrow in **d**). The cause of hydrocephalus in this patient is decompensated congenital aqueductal occlusion, which can be visualized in CISS images (arrowhead in **d**). Missing flow void phenomenon indicating occlusion. Evans' index (d1 / d2 in e) is abnormal (normal < 0.3).

of the corpus callosum and the floor of the third ventricle must be observed here (▶ **Fig. 1**). In the case of hydrocephalus, the corpus callosum bows upward and is thinned in the case of a persistent increase in pressure. The floor of the third ventricle is usually bowed upward. However, in the case of hydrocephalus, it is thinned or even bowed downward. Moreover, the infundibular recess is dilated with respect to the pituitary gland (▶ **Fig. 1**). The aqueduct should be evaluated on these scans with respect to possible obstructions.

Pulsation of the CSF through the aqueduct can be evaluated qualitatively on the basis of the flow void phenomenon on flow-sensitive T2w scans. Therefore, these should be included in the imaging protocol in addition to high-resolution sequences. Phase contrast (PC) examinations that allow dynamic imaging of CSF pulsation but only limited conclusions regarding anatomy can be alternatively used here. PC measurements perpendicular to the aqueduct also allow quantitative evaluation of CSF pulsation through the aqueduct [18]. The diagnostic value of these examination methods is controversial in the literature [19, 20]. An overview of the diagnostic criteria [12, 21] of hydrocephalus is provided in ▶ **Table 2**.

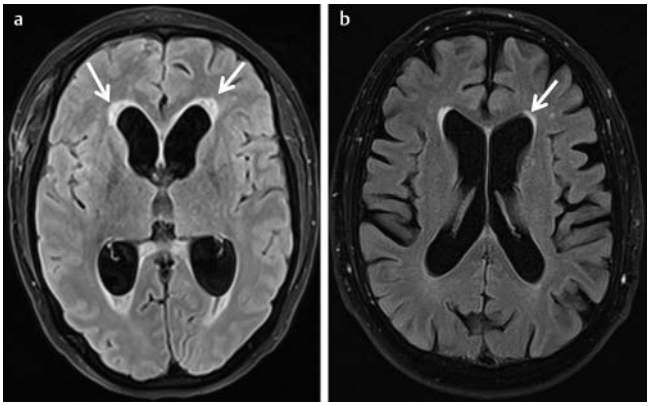

▶ **Fig. 2** Morphological imaging features of hydrocephalus. **a** Axial FLAIR image of a 43-year-old female patient with a three-week history of headache, nausea and vomiting. Hyperintense periventricular caps at the level of both frontal horns (arrow) indicating transependymal CSF extravasation with dilated ventricles due to hydrocephalus caused by posterior fossa metastasis. **b** Axial FLAIR image of a 59-year-old female patient with hearing loss on the right side. MRI was performed to exclude a tumor. Age-related periventricular white matter changes (arrow) in the area of the two frontal horns have to be differentiated from CSF extravasation.

Types of hydrocephalus

In principle, there are three different types of hydrocephalus, with normal pressure hydrocephalus having special classification as a fourth type.

Obstructive hydrocephalus

This type of hydrocephalus is also referred to as non-communicating hydrocephalus [6] and is caused by obstruction of CSF pathways. Although there are predilection sites for the obstruction of CSF pathways, it must be taken into consideration that in principle every intracranial tumor of a certain size can obstruct CSF pathways. Typical differential diagnoses for the various locations are listed in the following.

Foramen of Monro

A lesion in the region of the foramen of Monro can result in bilateral and more rarely unilateral dilatation of the lateral ventricles. The most common cause of an obstruction at this site is a colloid cyst. This is a benign, mucin-containing cyst that makes up approx. 1 % of all brain tumors and 20 % of all intraventricular masses [22]. These cysts are typically located on the roof of the third ventricle in the immediate vicinity of the foramen. They appear hyperdense on plain cranial CT. The cysts have a hyperintense signal in approx. 60 % of cases on T1-weighted (T1w) MRI scans. They are usually hypointense to isointense on T2w scans (▶ **Fig. 3**). Even if colloid cysts are histologically benign lesions, there is a risk of acute life-threatening hydrocephalus, e. g. due to an increase

This document was downloaded for personal use only. Unauthorized distribution is strictly prohibited.

▶ **Table 1** Imaging protocol.

	sequence						
	T1 MPR	**T2 TSE sagittal**	**T2 TSE axial**	**SE-DWI**	**T2 3D-CISS**	**TOF angiography**	**venous T1-weighted angiography**
slices	192	22	22	36	64	40	192
slice thickness (mm)	0.9	2	2	4	0.5	0.5	0.8
resolution (mm)	0.9 × 0.9	0.4 × 0.4	0.4 × 0.4	1.1 × 1.1	0.5 × 0.5	0.5 × 0.5	0.4 × 0.4
TR (ms)	1900	5000	5000	4200	1000	22	12
TE (ms)	2.58	82	82	95	132	3.6	5.1
TI (ms)	900						900
NEX	1	2.16	2.16	2	2	1	1
PAT factor	2	2	2	2	–	2	2
Gd administration	–	–	–	–	–	–	+
special feature			angled at lower edge of corpus callosum	diffusion factor b = 0/1000 s/mm²	angled over course of cranial nerve		reconstruction as MPR and MIP
measurement time (min)	2:16	2:16	2:16	1:00	4:50	5:48	7:06
						total measurement time:	25:32 min

MR imaging protocol at 3 T using a 32-channel head coil for signal detection for the diagnostic workup of patients with known hydrocephalus.
TR = repetition time, TE = echo time, TI = inversion time, TA = acquisition time, NEX = number of excitations, PAT factor = acceleration factor in parallel acquisition technique.

This document was downloaded for personal use only. Unauthorized distribution is strictly prohibited.

▶ **Table 2** Diagnostic criteria of hydrocephalus detected by imaging and the imaging modality allowing the best evaluation (mod. according to [12, 18]).

morphological imaging criterion	best evaluated on
dilated ventricular system; Evans' Index > 0.3	axial cranial CT axial T1w/T2w/FLAIR scans
dilated temporal horns	
rounded poster horns	
dilated third ventricle	
decreased mamillopontine distance	sagittal T2w scans
reduced frontal horn angle	
thinned and bowed corpus callosum	sagittal T2w scans
flattened cerebral sulcal pattern	axial T1w/T2w scans coronal T1 / T2w scans
transependymal CSF extravasation	axial cranial CT axial T2w/FLAIR scans
prominent "flow void" signal in the aqueduct (in NPH)	sagittal flow-sensitive T2w scans

in the size of the cyst [23]. Therefore, neurosurgical examination should be performed [24].

Obstruction of the foramen of Monro can also be caused by primary brain tumors, inflammatory changes, and the formation of septa (▶ **Fig. 4**) [25, 26]. The signal and contrast behavior of the tumor depends on entity and degree of malignancy. If the hydrocephalus is caused by a tumor, the imaging protocol should always include contrast-enhanced T1w scans on at least two perpendicular planes. Alternatively, contrast-enhanced T1w 3 D sequences (e. g. T1 MPR) can be used.

The formation of septa can be best evaluated on high-resolution T2w scans with these preferably being acquired/reconstructed in axial or coronal slice orientation.

Aqueduct

An acquired aqueduct stenosis is responsible for hydrocephalus in adults in up to 10 % of cases. Inflammatory septa and membranes in the aqueduct [1] and neurocysticercosis [27] are some of the most common causes. In particular, membranes and septa can be evaluated particularly effectively in high-resolution T2w sequences. However, aqueduct stenosis can also be caused by a process in the pineal gland region or a tectal tumor. The latter is usually a focal glioma. These are typically isodense on plain cranial CT and do not show any contrast enhancement. MRI is the method of choice for precise evaluation of tumor size [28]. These tumors appear hypointense to isointense on T1w scans and discretely hyperintense on T2w scans (▶ **Fig. 5**). Since these are usually low-grade tumors, they are not enhanced by contrast agent [29]. In the case of tumors with exophytic growth, a tumor of the pineal gland should be included in the differential diagnosis.

Pineal gland cysts [22], which are a common incidental finding in the daily diagnostic routine [30], are significantly more common. These are non-neoplastic glial cysts of the pineal region. In the case of giant pineal gland cysts, compression of the aqueduct or displacement of the ostium can be seen (▶ **Fig. 5**). However, an intermittent increase in size with secondary aqueduct stenosis and resulting hydrocephalus can occur in smaller cysts due to a valve mechanism [22]. Pineal gland cysts appear as masses that have smooth borders and are isodense to slightly hyperdense compared to CSF in CT and can have calcifications in the cyst wall [31]. The cyst contents are isointense to slightly hyperintense on T1w scans and CSF-isointense on T2w scans. Incomplete signal suppression is seen on FLAIR scans. Since the pineal gland does not have a blood-brain barrier, linear peripheral contrast enhancement is typically seen in CT and MRI. This can be nodular in up to 40 % of cases [22].

CT or MRI can be performed as initial imaging. However, since the exact position in relation to the aqueduct and tectum can be best evaluated on high-resolution T2-weighted sagittal scans, MRI is the examination modality of choice. Therefore, MRI should always be used for follow-up scans. To precisely evaluate the position of the cyst in relation to the tectum and aqueduct (▶ **Fig. 5**), high-resolution sagittal T2w sequences (e. g. CISS method) should be acquired. Contrast agent administration is not required for diagnosis.

Fourth ventricle and foramen magnum

In adults, the most common mass in the posterior cranial fossa that can result in compression of the fourth ventricle is a subacute cerebellar infarction [32] with consecutive swelling of the brain (▶ **Fig. 6**). On cranial CT, an infarction appears as a hypodense lesion in the supply area of the corresponding cerebellar artery. A hemorrhagic transformation can occur in the further course causing the infarction to appear partially hyperdense. Ischemic lesions appear hypointense on T1w MRI scans and hyperintense on T2w scans. Hemorrhagic changes can be evaluated most effectively on T2*w scans. In diffusion imaging, there is a signal increase on the diffusion-weighted scans in the acute phase with lowering of the values in the ADC parameter map. The most common neoplastic cause is intra-axial metastases (▶ **Fig. 6**) or, more rarely, primary brain tumors [32, 33]. The appearance on cranial CT and MRI depends on the underlying tumor entity but, as a rule, any contrast agent can be used to enhance the tumors [32].

The most common causes for compression on the level of the foramen magnum are congenital malformations of the base of the skull and of the craniocervical junctions and Chiari malformations [21], with these clinical pictures rarely first manifesting in adulthood.

Malabsorptive hydrocephalus

This form of hydrocephalus is caused by impaired CSF absorption. All ventricles are equally affected. Therefore, this type of hydrocephalus is also referred to as communicating hydrocephalus. It can be caused by subarachnoid bleeding (SAB) or posthemorrhagic changes after SAB as well as inflammatory or post-inflammatory changes (▶ **Fig. 7**). Moreover, malabsorptive hydrocephalus can

This document was downloaded for personal use only. Unauthorized distribution is strictly prohibited.

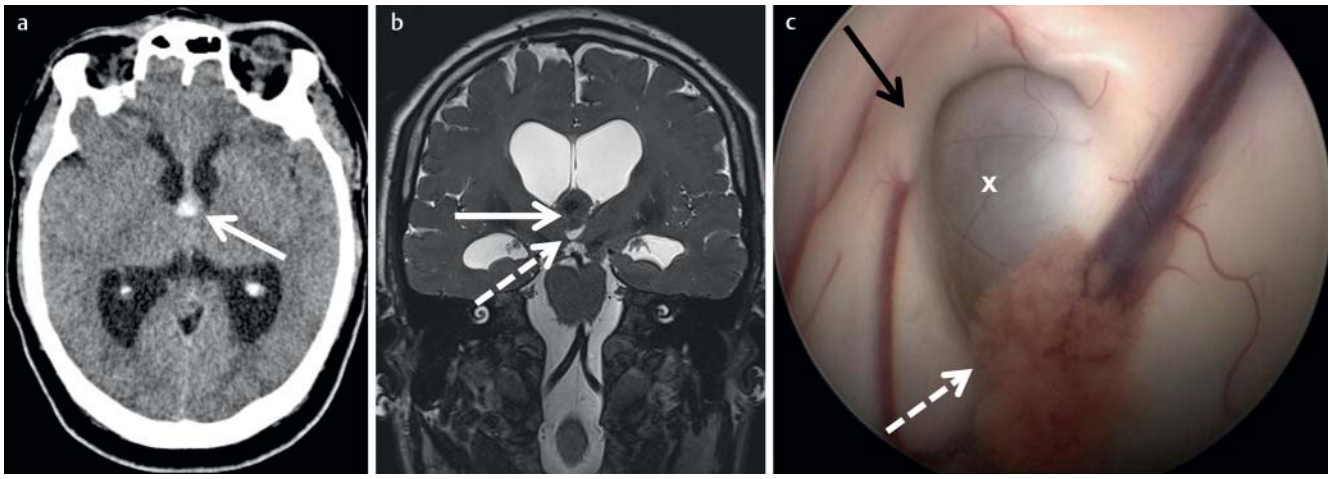

▶ **Fig. 3** Colloid cyst. **a** Axial plain cranial CT scan of a 56-year-old patient with a two-day history of headache, nausea and vomiting. Hydrocephalus with bilateral dilatation of the posterior horns of the lateral ventricle due to a colloid cyst (arrow). The cyst typically appears hyperdense on plain CT. **b** Coronal CISS image at the level of the foramen of Monro of a 44-year-old patient with bilateral hydrocephalus. Bilateral obstruction of the foramen by a colloid cyst (arrow) in the foramen. The cyst appears hypointense and the third ventricle (dotted arrow) is small and distorted by the cyst. **c** Intraoperative endoscopic view from the right frontal horn of a 43-year-old patient with hydrocephalus due to a colloid cyst. Obstruction of the foramen (black arrow) by the colloid cyst (x). Dotted arrow indicates choroid plexus.

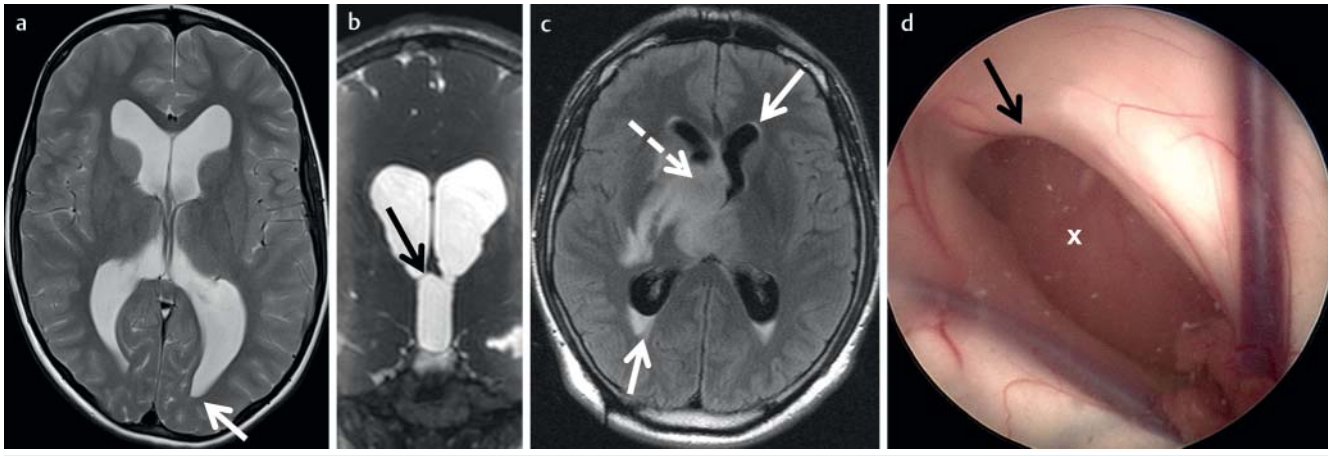

▶ **Fig. 4** Obstructive hydrocephalus due to obstruction of the foramen of Monro. **a** Axial T2-weighted image of a 54-year-old female patient with a 5-year history of headache and acute worsening. Dilated posterior horns of the lateral ventricles on both sides (arrow). **b** Coronal CISS image of the same patient. Hydrocephalus is caused by post-infectious membranes (arrow) at the level of the foramen of Monro on both sides. **c** Axial FLAIR image of a 39-year-old patient with a several day history of headache. Occlusive hydrocephalus with CSF extravasation around the frontal and occipital horns (arrows) due to a tumor at the level of the foramen of Monro and the thalamus (dotted arrow). **d** Intraoperative endoscopic view of the tumor (x) from the left frontal horn through the foramen of Monro (black arrow). Histologically proven pilocytic astrocytoma.

also develop as part of meningism in a malignant primary disease. The hydrocephalus can be acute as well as slowly progressing. SAB is usually caused by rupture of an aneurysm of the arteries supplying the brain and is accompanied by the typical symptoms with abrupt onset of headache. Subarachnoid bleeding appears hyperdense on plain cranial CT in the region of the basal cisterns [30] and hydrocephalus can represent an acute complication of the disease. Moreover, acute occlusive hydrocephalus can occur in SAB due to clots. In the case of slowly developing post-hemorrhagic hydrocephalus, blood residues typically can no longer be detected on cranial CT so that the patient's history is decisive for the correct diagnosis. In contrast, post-hemorrhagic changes can be detected on T2*w MRI scans for a much longer period of time.

Inflammatory intracranial processes are usually serious and patients have a systemic reaction with fever and headache. Inflammatory changes can be detected more effectively on MRI and cranial CT [34]. In the case of meningitis, significant enhancement in the region of the meninges can be seen after contrast administration in MRI. Encephalitis is usually associated with a cortical and subcortical signal increase that can be detected particularly effectively on FLAIR scans and diffusion-weighted images. In addition, a lack of signal suppression in the region of the CSF can be detected on FLAIR scans in the area of the inflam-

This document was downloaded for personal use only. Unauthorized distribution is strictly prohibited.

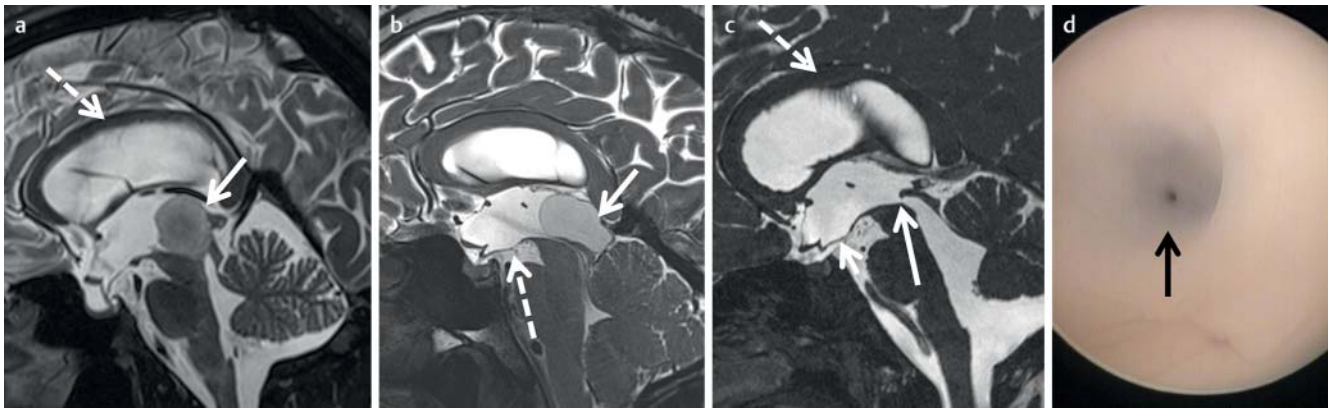

▶ **Fig. 5** Typical causes of aqueductal obstruction. **a** Sagittal CISS image of a 24-year-old female patient with a 6-month history of headache and eye movement disturbances demonstrating a hyperintense tectal mass with obstruction of the aqueduct. Consecutive hydrocephalus with upward bowing of the corpus callosum (dotted arrow), while the floor of the third ventricle is pushed downward. **b** Sagittal T2w SPACE image of a 28-year-old patient with a 4-month history of morning vomiting. Giant pineal gland cyst (arrow) compressing the aqueduct and obstructing its entrance. Downward bowing of the floor of the third ventricle indicating hydrocephalus (dotted arrow). **c** Sagittal CISS image of a 43-year-old female patient with a 4-month history of headache. Aqueductal stenosis (arrow) at the level of the inlet. Upward bowing and mild thinning of the corpus callosum (dotted arrow) and downward bowing of the floor of the third ventricle (arrow head) indicating hydrocephalus. **d** Intraoperative endoscopic view of the same patient as in **c** demonstrating the pinhole configuration of the aqueduct (arrow).

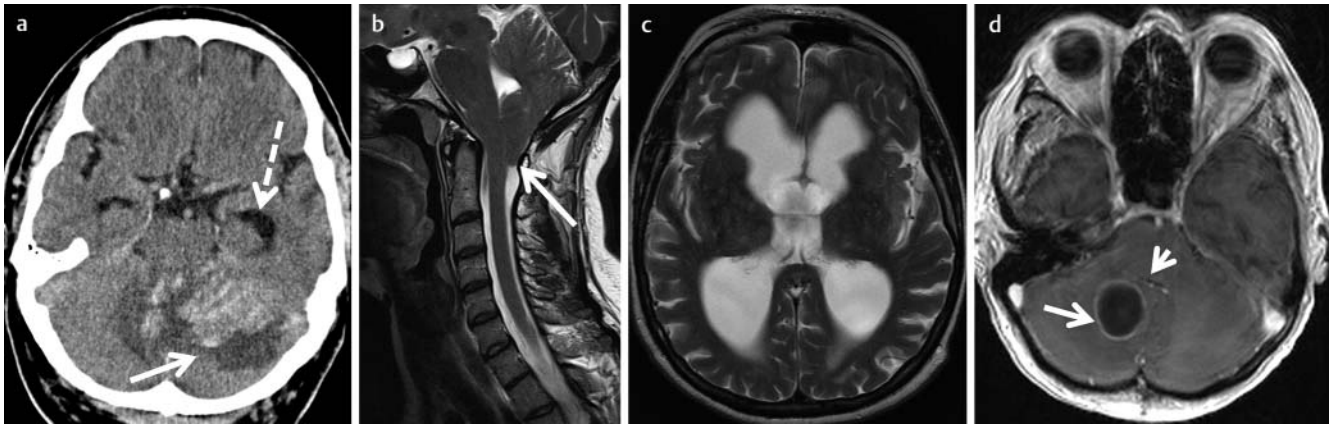

▶ **Fig. 6** Obstruction in the posterior fossa. **a** Plain cranial CT scan of a 75-year-old patient with hemorrhagic transformation of bilateral infarcts in the PICA territory (arrow) with compression of the fourth ventricle. Acute hydrocephalus is indicated by dilatation of both temporal horns (dotted arrow). **b** Sagittal T2w image of a 27-year-old female patient with a long history of headache and difficulties concentrating. The tip of the cerebellar tonsils is below the foramen magnum, indicating Chiari I malformation as the cause of hydrocephalus. **c** Axial T2w image of the same patient as in **b** demonstrating ventriculomegaly as a sign of chronic hydrocephalus. **d** Axial contrast-enhanced T1w image of a 64-year-old female patient with a ring-enhancing lesion (arrow) compressing the forth ventricle (arrowhead) (lung cancer metastasis).

matory changes. Contrast enhancement can be detected both in the arachnoid space and in the region of the dura mater. In immunocompromised patients, some inflammatory changes can be visualized better on high-resolution T2w scans (▶ **Fig. 7**) than on contrast-enhanced scans [34, 35]. Since the imaging findings are often unclear, a correlation with clinical symptoms and lumbar puncture with CSF diagnostic testing are important for correct diagnosis [35]. Particularly in inflammatory processes, it must be taken into consideration that hydrocephalus can progress quickly [35].

Hypersecretory hydrocephalus

This type of hydrocephalus is caused by an overproduction of CSF, which is usually caused by a plexus papilloma (▶ **Fig. 8**) or more rarely by a plexus carcinoma [36]. These are typically tumors in children. On plain cranial CT, the tumors appear isodense with respect to the brain parenchyma. On MRI the tumor appears lobulated. It is isointense to hypointense with respect to the brain on T1w scans and isointense to hyperintense on T2w scans. After contrast administration significant enhancement is seen. On T2w scans flow void phenomena caused by tumor vessels can be

This document was downloaded for personal use only. Unauthorized distribution is strictly prohibited.

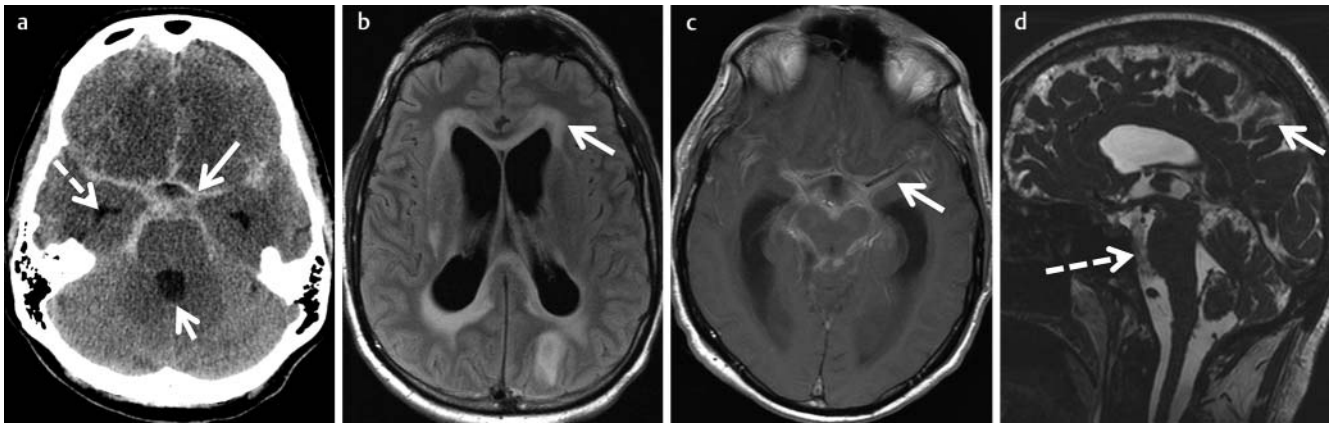

▶ **Fig. 7** Typical differential diagnoses of malbsorptive hydrocephalus. **a** 54-year-old female patient with sudden onset of severe headache; plain cranial CT scan demonstrating extensive subarachnoid hemorrhage (SAH) in the basal cistern (arrow) with concomitant hydrocephalus and bilaterally dilated temporal horns (dotted arrow) and fourth ventricle (arrowhead). **b** Axial FLAIR image of a 56-year-old patient with a 6-week history of cough and acute headache. Extensive acute hydrocephalus with transependymal CSF extravasation at the level of the frontal (arrow) and occipital horns. **c** Axial postcontrast T1w image of the same patient demonstrating extensive subarachnoid enhancement due to tuberculous meningitis. **d** Sagittal CISS image of a 43-year-old female patient with headache and severe neutropenia. CSF analysis revealed Hemophilus influenza meningitis. Extensive infectious CSF changes in the prepontine cistern (dotted arrow) and in the hemispheres. Contrast-enhanced images demonstrated no blood-brain-barrier breakdown due to neutropenia.

detected within the tumor. Intratumoral calcifications can be evaluated on MRI, particularly in T2*w gradient echo MRI sequences.

Idiopathic normal pressure hydrocephalus

Idiopathic normal pressure hydrocephalus (iNPH) is a special type of communicating hydrocephalus whose pathophysiology is not yet fully understood. The disease typically occurs in adults and the prevalence increases with age [37, 38]. It is primarily caused by impaired CSF dynamics with no or only a slight increase in intracranial pressure [37]. iNPH is defined by typical clinical and radiological criteria. Typical clinical symptoms are gait disturbance, urine incontinence and dementia (Hakim's triad [38]), the full clinical picture being seen in only approx. 30 % of all patients. Correct diagnosis is particularly important since iNPH is a treatable form of dementia. In the case of corresponding clinical suspicion, MRI is the examination modality of choice. Typical radiological criteria are ventricular dilatation and small external CSF spaces above the hemispheres without additional signs of an increase in intracranial pressure. These changes can be best evaluated on coronal images (▶ **Fig. 9**) [39]. Moreover, dilated cerebral sulci can be seen in isolated cases in patients with iNPH and can further support the diagnosis as a further morphological imaging criterion in the overall context. A very prominent flow void phenomenon in the region of the aqueduct is an indication of impaired CSF dynamics on sagittal T2w scans (▶ **Fig. 9**). Impaired CSF dynamics can be visualized and quantified with the help of phase contrast scans [38]. However, the relevance of these findings for diagnosis and the prediction of treatment response is controversial in the literature [19, 20].

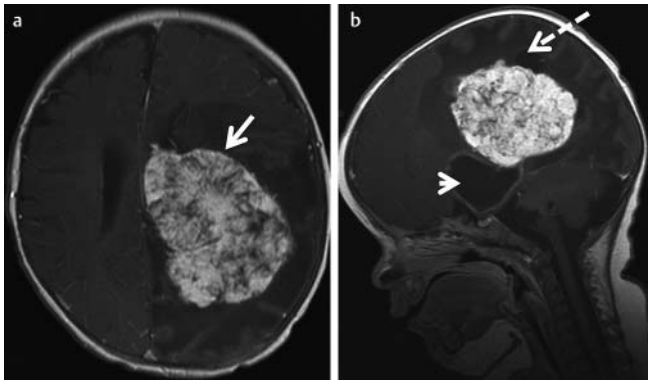

▶ **Fig. 8** MRI of an 8-year-old patient with a rapidly enlarging head due to plexus papilloma (arrow in **a**) with subsequent dilatation of the temporal horn (arrowhead in **b**) and trigone (dotted arrow in **b**).

Differential diagnoses

Hydrocephalus must be differentiated from other diseases associated with an increase in intracranial pressure and from changes resulting in ventricular dilatation.

Idiopathic intracranial hypertension

In idiopathic intracranial hypertension (IIH), there is an increase in intracranial pressure without a morphological intracranial pathology visible on imaging [40]. This must be differentiated from pseudotumor cerebri, which is often used synonymously [41] and refers to an increase in intracranial pressure with a definable cause (▶ **Table 3**) [40]. IIH primarily affects overweight women of childbearing age. Typical clinical symptoms are headache, vision impairment or loss of field of vision, pulsatile tinnitus, and neck pain. Diagnosis is based on the modified Dandy criteria (▶ **Table 4**) [41]. On cranial CT, pathologies often cannot be

This document was downloaded for personal use only. Unauthorized distribution is strictly prohibited.

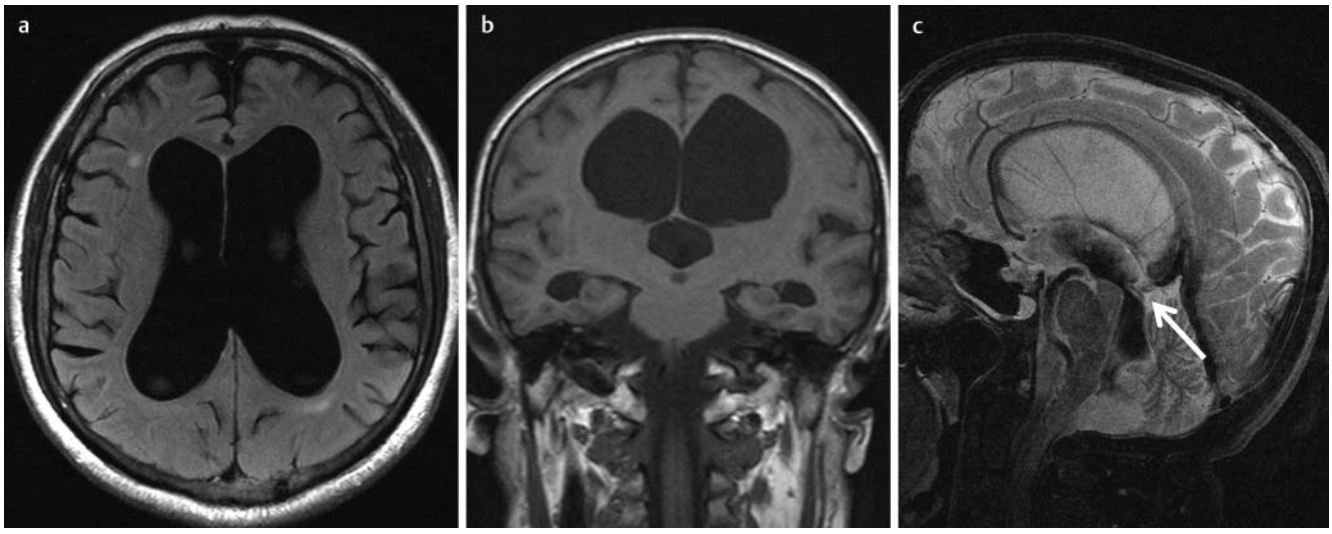

▶ **Fig. 9** 63-year-old patient with progressive gait disturbance, mild cognitive impairment and urinary incontinence. **a** Axial FLAIR image demonstrating ventriculomegaly without evidence of transependymal CSF extravasation. **b** Coronal T1w image demonstrating mismatch between size of inner and outer CSF spaces. **c** Flow-sensitive sagittal T2w image demonstrating strong flow void in the aqueduct as an indirect sign of iNPH.

▶ **Table 3** Causes of pseudotumor cerebri (mod. according to [37]).

associated diseases	iatrogenic
anemia	antibiotic therapy (tetracycline [minocycline; doxycycline]; nitrofurantoin; sulfonamides; quinolones [nalidixic acid])
hormonal disorder (Addison's disease; Cushing's disease)	hormonal factors (L-thyroxine; growth hormone; tamoxifen)
sleep apnea	excessive intake of vitamin A; retinoids
hypercapnia	medication (corticosteroids; lithium, ciclosporin)
trisomy 21; Turner syndrome	
kidney failure	
autoimmune diseases (systemic erythematosus lupus; Sjögren's syndrome)	

▶ **Table 4** Modified Dandy criteria for diagnosis of idiopathic intracranial hypertension (mod. according to [38]). For reliable diagnosis, criteria A-E have to be satisfied and no secondary cause should be present. For a probable diagnosis of IIH, criteria A-D must be fulfilled.

A	papilledema in fundoscopy
B	normal neurological examination, except for affection of cranial nerves
C	normal cerebral imaging[1]: no sign of hydrocephalus (▶ **Table 1**), no tumor or structural lesion, no pathological meningeal enhancement, no evidence of sinus/venous thrombosis
D	normal CSF analysis
E	increased CSF pressure in lumbar puncture in side position (> 25 cm H_2O)

[1] Imaging modality of choice is MRI; if not possible, contrast-enhanced cranial CT can be performed.

detected in axial slice orientation. Therefore, MRI is the preferred examination modality. Typical morphological imaging findings (▶ **Fig. 10**) are thinning of the pituitary gland tissue (empty sella sign), dilatation of the CSF spaces around the optic nerve with or without accompanying tortuosity of the nerve, thinning of the dorsal circumference of the eyeball, a prominent papilla of the optic nerve, and stenosis of the transverse sinus [40 – 42]. Therefore, in the case of corresponding clinical suspicion, the imaging

This document was downloaded for personal use only. Unauthorized distribution is strictly prohibited.

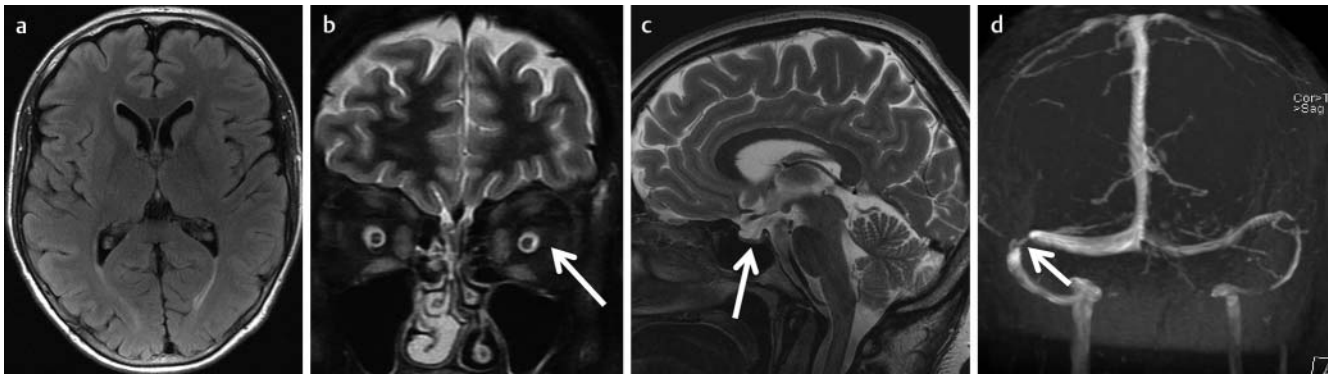

▶ **Fig. 10** 27-year-old obese female patient with headache and visual disturbances for 3 months. Cranial MRI demonstrates the typical signs of pseudotumor cerebri. **a** Axial FLAIR images without evidence of hydrocephalus. **b** Sagittal T2w image with thinning (arrow) of the pituitary gland (empty sella sign). **c** Coronal fat-saturated T2w showing dilatation of the CSF spaces around the optic nerve (arrow). **d** CE-MRA demonstrating stenosis of the right transverse sinus (arrow) and hypoplastic left transverse sinus. Image findings resolved after lumbar puncture.

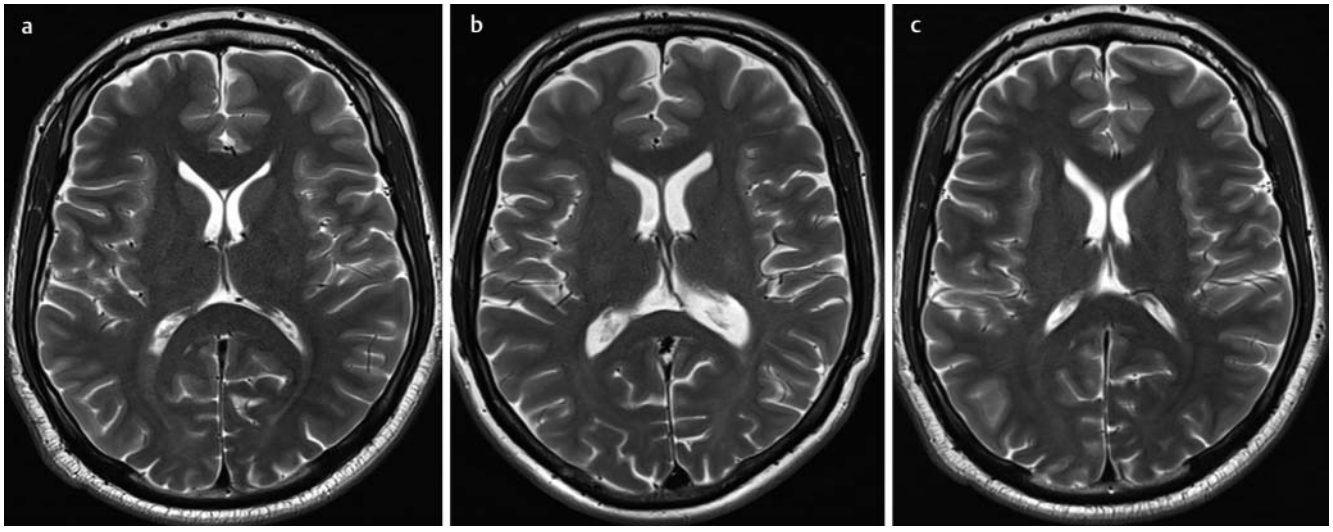

▶ **Fig. 11** Secondary atrophy due to dehydration. Axial T2w images of a 43-year-old patient. **a** Initial MRI performed to exclude intracranial complications of sinusitis. **b** Follow-up MRI which was performed after the patient collapsed at a sports event due to exsiccosis. Dilatation of inner and outer CSF spaces. **c** Follow-up MRI three days later after rehydration demonstrating normalization of the CSF spaces.

protocol should include venous angiography either using the "time of flight" (TOF) technique or preferably as contrast-enhanced MR venography (CE-MRV) [42]. The described changes after lumbar puncture are typically fully reversible [40].

Age-related changes

A physiological reduction in brain volume occurs with increasing age. However, in contrast to hydrocephalus, there is symmetrical dilatation of internal and external CSF spaces. Age-related cortical atrophy primarily relates to the sensomotoric cortex, the visual occipital cortex, individual frontal areas and the thalamus [15]. Pathological atrophy as can occur, for example, in dementia must be differentiated from this. While ventricular dilatation due to subcortical atrophy is non-specific, certain types of cortical atrophy allow conclusions regarding the primary disease, e. g., hippocampus atrophy in Alzheimer's [43]. However, in the individual case, differentiation can be difficult. Therefore, a correlation of imaging findings with symptoms is essential for correct interpretation [43]. The diagnostic reliability for the differentiation of physiological age-related changes from hydrocephalus can be increased by using age-specific reference images [44].

Secondary atrophy

Hydrocephalus must also be differentiated from secondary atrophy as can occur, for example, in autoimmune diseases [45], HIV infection [46], after chemotherapy [47], in neurodegenerative diseases [15], or after taking drugs or medications [48]. Dehydration [49] can also lead to temporary ventricular dilatation (▶ **Fig. 11**). As in aging processes, symmetrical dilatation of the internal and external CSF spaces occurs. For correct interpretation of findings, correlation with symptoms and the particular patient history is extremely important.

This document was downloaded for personal use only. Unauthorized distribution is strictly prohibited.

Summary

In hydrocephalus, an imbalance between CSF production and absorption or obstruction of CSF pathways results in ventricular dilatation and consecutively in increased intracranial pressure. Acute hydrocephalus is a life-threatening disease and requires urgent neurosurgical treatment. It can be caused by an obstruction (occlusive hydrocephalus) of CSF circulation or impaired absorption (malabsorptive hydrocephalus). Hydrocephalus must be differentiated from ventricular dilatation due to age or secondary atrophy. Imaging is essential to identify the cause in occlusive hydrocephalus so that treatment can be planned.

Conflict of Interest

The authors declare that they have no conflict of interest.

References

[1] Kahle KT, Kulkarni AV, Limbrick DD Jr et al. Hydrocephalus in children. Lancet (London, England) 2016; 387: 788 – 799

[2] Reith W, Yilmaz U. Hydrocephalus and intracranial hypotension. Der Radiologe 2012; 52: 821 – 826

[3] Symss NP, Oi S. Theories of cerebrospinal fluid dynamics and hydrocephalus: historical trend. Journal of neurosurgery Pediatrics 2013; 11: 170 – 177

[4] Eymann R. Clinical symptoms of hydrocephalus. Der Radiologe 2012; 52: 807 – 812

[5] Sakka L, Coll G, Chazal J. Anatomy and physiology of cerebrospinal fluid. European annals of otorhinolaryngology, head and neck diseases 2011; 128: 309 – 316

[6] Greitz D. Radiological assessment of hydrocephalus: new theories and implications for therapy. Neurosurgical review 2004; 27: 145 – 165 discussion 166-147

[7] Brinker T, Stopa E, Morrison J et al. A new look at cerebrospinal fluid circulation. Fluids and barriers of the CNS 2014; 11: 10

[8] Bulat M, Klarica M. Recent insights into a new hydrodynamics of the cerebrospinal fluid. Brain research reviews 2011; 65: 99 – 112

[9] Oreskovic D, Klarica M. The formation of cerebrospinal fluid: nearly a hundred years of interpretations and misinterpretations. Brain research reviews 2010; 64: 241 – 262

[10] Preuss M, Hoffmann KT, Reiss-Zimmermann M et al. Updated physiology and pathophysiology of CSF circulation – the pulsatile vector theory. Child's nervous system – official journal of the International Society for Pediatric Neurosurgery 2013; 29: 1811 – 1825

[11] Fink KR, Benjert JL. Imaging of Nontraumatic Neuroradiology Emergencies. Radiologic clinics of North America 2015; 53: 871 – 890, x

[12] Kartal MG, Algin O. Evaluation of hydrocephalus and other cerebrospinal fluid disorders with MRI: An update. Insights into imaging 2014; 5: 531 – 541

[13] LeMay M, Hochberg FH. Ventricular differences between hydrostatic hydrocephalus and hydrocephalus ex vacuo by computed tomography. Neuroradiology 1979; 17: 191 – 195

[14] Ragan DK, Cerqua J, Nash T et al. The accuracy of linear indices of ventricular volume in pediatric hydrocephalus: technical note. Journal of neurosurgery Pediatrics 2015; 15: 547 – 551

[15] Pini L, Pievani M, Bocchetta M et al. Brain atrophy in Alzheimer's Disease and aging. Ageing research reviews 2016; 30: 25 – 48

[16] Kim H, Jeong EJ, Park DH et al. Finite element analysis of periventricular lucency in hydrocephalus: extravasation or transependymal CSF absorption? Journal of neurosurgery 2016; 124: 334 – 341

[17] Kartal MG, Ocakoglu G, Algin O. Feasibility of 3-dimensional sampling perfection with application optimized contrast sequence in the evaluation of patients with hydrocephalus. Journal of computer assisted tomography 2015; 39: 321 – 328

[18] Bradley WG Jr. Magnetic Resonance Imaging of Normal Pressure Hydrocephalus. Seminars in ultrasound, CT, and MR 2016; 37: 120 – 128

[19] Jaeger M, Khoo AK, Conforti DA et al. Relationship between intracranial pressure and phase contrast cine MRI derived measures of intracranial pulsations in idiopathic normal pressure hydrocephalus. Journal of clinical neuroscience – official journal of the Neurosurgical Society of Australasia 2016; 33: 169 – 172

[20] Qvarlander S, Ambarki K, Wahlin A et al. Cerebrospinal fluid and blood flow patterns in idiopathic normal pressure hydrocephalus. Acta neurologica Scandinavica 2016. DOI: 10.1111/ane.12636

[21] Dincer A, Ozek MM. Radiologic evaluation of pediatric hydrocephalus. Child's nervous system – official journal of the International Society for Pediatric Neurosurgery 2011; 27: 1543 – 1562

[22] Osborn AG, Preece MT. Intracranial cysts: radiologic-pathologic correlation and imaging approach. Radiology 2006; 239: 650 – 664

[23] Beaumont TL, Limbrick DD Jr, Rich KM et al. Natural history of colloid cysts of the third ventricle. Journal of neurosurgery 2016; 125: 1420 – 1430

[24] Langner S, Buelow R, Fleck S et al. Management of Intracranial Incidental Findings on Brain MRI. Fortschr Röntgenstr 2016; 188: 1123 – 1133

[25] Schroeder HW, Oertel J, Gaab MR. Endoscopic treatment of cerebrospinal fluid pathway obstructions. Neurosurgery 2007; 60: ONS44 – ONS51; discussion ONS51-42

[26] Vaz-Guimaraes Filho FA, Ramalho CO, Suriano IC et al. Neuroendoscopic surgery for unilateral hydrocephalus due to inflammatory obstruction of the Monro foramen. Arquivos de neuro-psiquiatria 2011; 69: 227 – 231

[27] Webb CM, White AC Jr. Update on the Diagnosis and Management of Neurocysticercosis. Current infectious disease reports 2016; 18: 44

[28] Boydston WR, Sanford RA, Muhlbauer MS et al. Gliomas of the tectum and periaqueductal region of the mesencephalon. Pediatric neurosurgery 1991; 17: 234 – 238

[29] Igboechi C, Vaddiparti A, Sorenson EP et al. Tectal plate gliomas: a review. Child's nervous system – official journal of the International Society for Pediatric Neurosurgery 2013; 29: 1827 – 1833

[30] Langner S, Kirsch M. Radiological Diagnosis and Differential Diagnosis of Headache. Fortschr Röntgenstr 2015; 187: 879 – 891

[31] Lensing FD, Abele TA, Sivakumar W et al. Pineal region masses – imaging findings and surgical approaches. Current problems in diagnostic radiology 2015; 44: 76 – 87

[32] Grossman R, Ram Z. Posterior Fossa Intra-Axial Tumors in Adults. World neurosurgery 2016; 88: 140 – 145

[33] Shih RY, Smirniotopoulos JG. Posterior Fossa Tumors in Adult Patients. Neuroimaging clinics of North America 2016; 26: 493 – 510

[34] Rath TJ, Hughes M, Arabi M et al. Imaging of cerebritis, encephalitis, and brain abscess. Neuroimaging clinics of North America 2012; 22: 585 – 607

[35] Sarrazin JL, Bonneville F, Martin-Blondel G. Brain infections. Diagnostic and interventional imaging 2012; 93: 473 – 490

[36] Shi YZ, Wang ZQ, Xu YM et al. MR findings of primary choroid plexus papilloma of the cerebellopontine angle: report of three cases and literature reviews. Clinical neuroradiology 2014; 24: 263 – 267

[37] Lieb JM, Stippich C, Ahlhelm FJ. Normal pressure hydrocephalus. Der Radiologe 2015; 55: 389 – 396

This document was downloaded for personal use only. Unauthorized distribution is strictly prohibited.

[38] Picascia M, Zangaglia R, Bernini S et al. A review of cognitive impairment and differential diagnosis in idiopathic normal pressure hydrocephalus. Functional neurology 2015; 30: 217 – 228

[39] Kitagaki H, Mori E, Ishii K et al. CSF spaces in idiopathic normal pressure hydrocephalus: morphology and volumetry. AJNR American journal of neuroradiology 1998; 19: 1277 – 1284

[40] Markey KA, Mollan SP, Jensen RH et al. Understanding idiopathic intracranial hypertension: mechanisms, management, and future directions. The Lancet Neurology 2016; 15: 78 – 91

[41] Friedman DI, Liu GT, Digre KB. Revised diagnostic criteria for the pseudotumor cerebri syndrome in adults and children. Neurology 2013; 81: 1159 – 1165

[42] Bidot S, Saindane AM, Peragallo JH et al. Brain Imaging in Idiopathic Intracranial Hypertension. Journal of neuro-ophthalmology 2015; 35: 400 – 411

[43] Bakkour A, Morris JC, Wolk DA et al. The effects of aging and Alzheimer's disease on cerebral cortical anatomy: specificity and differential relationships with cognition. NeuroImage 2013; 76: 332 – 344

[44] Richards JE, Sanchez C, Phillips-Meek M et al. A database of age-appropriate average MRI templates. NeuroImage 2016; 124: 1254 – 1259

[45] Filippi M. MRI measures of neurodegeneration in multiple sclerosis: implications for disability, disease monitoring, and treatment. Journal of neurology 2015; 262: 1 – 6

[46] Holt JL, Kraft-Terry SD, Chang L. Neuroimaging studies of the aging HIV-1-infected brain. Journal of neurovirology 2012; 18: 291 – 302

[47] Arrillaga-Romany IC, Dietrich J. Imaging findings in cancer therapy-associated neurotoxicity. Seminars in neurology 2012; 32: 476 – 486

[48] Rojas R, Riascos R, Vargas D et al. Neuroimaging in drug and substance abuse part I: cocaine, cannabis, and ecstasy. Topics in magnetic resonance imaging 2005; 16: 231 – 238

[49] Dickson JM, Weavers HM, Mitchell N et al. The effects of dehydration on brain volume – preliminary results. International journal of sports medicine 2005; 26: 481 – 485

This document was downloaded for personal use only. Unauthorized distribution is strictly prohibited.